Title

High colloidal stability of gold nanorods coated with a peptide-ethylene glycol: analysis by cyanide-mediated etching and nanoparticle tracking analysis.

Paul Free*[a], Gao Conger[b], Wu Siji[a], Jing Bo Zhang[c], David G. Fernig[d].

[a]Institute of Materials Research and Engineering, Agency for Science, Technology & Research (A*STAR), 2 Fusionopolis Way, Innovis, #08-03, Singapore 138634.
[b]Division of Bioengineering and [c]Advanced Environmental & Biotechnology Centre, Nanyang Environment & Water Research Institute, Nanyang Technological University, Singapore 637141.
[d]Department of Biochemistry, Institute of Integrative Biology, University of Liverpool, Liverpool L69 7ZB, UK.
***corresponding author: freepf@imre.a-star.edu.sg**

Total Words: 5482.
Number of Figures: 5.

Abstract

The stability of gold nanorods was assessed following coating with various charged or uncharged ligands, mostly peptides. Highly stable monodispersed gold nanorods were obtained by coating CTAB-stabilized gold nanorods with a pentapeptide with C-terminal ethylene glycol units (peptide-EG). UV-vis spectroscopy of these nanorods suspended in saline solutions indicated no signs of aggregation, and they were easily purified using size-exclusion chromatography. A more stringent measure of nanorod stability involved observing changes in the UV-vis absorbance of gold nanorods subjected to etching with cyanide. The λ_{max} absorbance of peptide-EG coated nanorods red-shifted in etchant solution. The hypothesis that changes in the nanorod aspect ratio led to this red-shift was confirmed by TEM analysis, which showed pit formation along the transverse axis. The etching process was followed in solution using nanoparticle tracking analysis. The red-shift was shown to occur while the particles remained mono-dispersed, and so was not due to aggregation. Adding both etchant solution and peptide-EG to the nanorods was further shown to allow modulation of the $\Delta\lambda_{max}$ red-shift and increase the etchant resistance of peptide-EG nanorods. Thus, very stable gold nanorods can be produced using the peptide-EG coating approach and their optical properties modulated with etchant.

Introduction

Gold nanorods (NRs) strongly absorb and scatter light in the UV-vis and near-infrared (NIR) range.[1–3] Example nanorod physical properties and property-associated applications include; 1) photoabsorption of NIR radiation for use in biomedical photothermal or photoacoustic therapy,[4–8] 2) a surface plasmon resonance (SPR) effect for nanorod sensitivity to environmental or morphology changes,[9] and 3) a surface-enhanced Raman effect for label-free detection of biomolecules.[10–12] These examples characterise a high sensitivity of NRs to the environment and molecules attaching to the surface of NRs. Colloidal stability is thus an important consideration for the use of NRs. Additionally, biocompatibility concerns exist with the use of NRs coated with hexadecyltrimethylammonium bromide (CTAB), a molecule known to exhibit cytotoxicity and typically coating their surface after most syntheses.[13] These issues are typically addressed by coating the NRs with an alternative molecular layer. There are many strategies for this, including encapsulating NRs with a silica shell, replacement of CTAB with polymers such as polyelectrolytes[14] or polyethylene glycols (PEGs),[15–18] or formation of self-assembled monolayers (SAMs) of thiolates containing terminal ethylene glycol units (EG), alkyl ligands or charged groups.[19–22] While such strategies are successful for stabilisation, there are some clear disadvantages. For example, polyelectrolyte-coated gold nanorods[14] are highly charged and, therefore, will bind non-specifically (in the biological sense) to biological polymers (proteins, polysaccharides, glycolipids, etc.) of the opposite charge. Such non-specific binding will alter their biological function in a non-predictable manner. The use of charged molecules to form SAMs on NRs have the same non-specific binding problem as for polyelectrolytes.[19,22–25]

While the PEG modification of nanorods is common and can impart excellent physical stability, a disadvantage of the use of PEGs in stabilising nanomaterials is that they result in a large increase in hydrodynamic radius. Thus, for applications that require a close association with the NR surface, e.g. surface-enhanced Raman scattering, a polymer, which will impart a greater hydrodynamic radius may interfere with this effect, whereas our peptide-EG SAMs of < 2 nm in length if fully extended, are likely not to. Moreover, in some instances with nanoparticles, it has been found that the polymer leaves substantial gaps, which allows small molecules access to the surface.[26] Consequently, ligand-exchange with small biological thiols, e.g., cysteine, glutathione, may be a problem in this case. It is also fairly challenging to functionalise PEG-coated nanomaterials. We have previously used SAMs of peptides, peptidols, and alkanethiol EGs[27,28] to coat noble-metal nanoparticles. These SAMs provides a good level of stability when applied to nanoparticles[29,30] and allow the control of chemical functionalization, the number of surface-attached molecules and control of surface charge.[31–34]

The effectiveness of a coating on colloidal noble-metal nanoparticles can be assessed by measuring their electrolyte-induced aggregation. However, more stringent tests are necessary if the material is to be considered for biosensor and biotechnology applications. Such tests include probing the susceptibility of the SAM to ligand exchange with small thiols (and subsequent destabilization of the particles),[29] or the resistance of the SAM to a metal etching reaction,[30] both of which provide insight into the packing of the SAM and the likelihood of biological molecules in a sensing scenario from destabilizing the nanoparticles. Etching has also been used to study NR anisotropy and chemical reactivity,[35–38] to change the shape (and thus optical properties) of NRs,[39–41] and for sensing.[42–45].

In this report, we tested different ligands for their ability for form a SAM on gold NRs that imparted good stability. We found that a pentapeptide-EG (peptide-EG) imparted the best stability to the NRs. For example, gold NRs coated with peptide-EG were far more resistant to etching. Surprisingly, in the presence of etchant, the λmax of the NRs red-shifted, while the particle concentration decreased slowly. Nanoparticle tracking demonstrated that at least over the first two hours of etching the NRs remained monodisperse, so the red-shift was not due to NR aggregation, though at later times (3h) there was evidence for aggregation. TEM analysis identified a transverse etching mechanism since pits were observed along the length of the NRs. By adding etchant and pentapeptide-EG to purified pentapeptide-EG coated NRs it was possible to control the redshift of the λmax and produce NRs with a higher resistance to etching. The peptide-EG used to coat NRs was inspired by the success of alkanethiol ethyleneglycol/peptidol SAMs we developed for gold nanoparticles, for which unequivocal evidence for specific biological targeting has been presented. Importantly, these nanoparticles have been used to solve biological problems.[46,47] Thus, peptide-EG ligands provide an important step forwards in the synthesis of gold NRs that have sufficient stability to be useful in biosensor and biotechnology applications.

Experimental

Materials

Peptides H-CALNN-OH, H-CVVVT-ol (T-ol is for threoninol) and H-CVVVT-NH-$(CH_2CH_2O)_4$-H (termed peptide-EG: Mw 695) were obtained from Peptide Protein Research Ltd (Fareham, UK). Ethylene glycol-derived alkanethiol, HS-$(CH_2)_{11}$-EG_6, Mw 468, was purchased from Prochimia (ProChimia Surfaces Sp. z o.o., Sopot, Poland). 600 nm λ_{max} wavelength (25 nm diameter, 49 nm length) and 808 nm λ_{max} wavelength (23 nm diameter, 85 nm length) gold nanorods were purchased from Nanopartz Inc. (Colorado, USA), and coated with < 100 mM CTAB. Gold (III) chloride trihydrate, hexadecyltrimethyl ammonium bromide (CTAB), silver nitrate, L-ascorbic acid, hydrochloric acid, sodium phosphate buffer (PBS: 8.1 mM Na_2HPO_4, 1.2 mM, KH_2PO_4, 140 mM NaCl, and 2.7 mM KCl, pH 7.4), sodium chloride, 1,4-dithiothreitol (DTT), sodium borohydride, sodium hydroxide and sodium cyanide were obtained from Sigma Aldrich Pte Ltd (Singapore). Note that sodium cyanide is highly toxic, and must not be used in acidic solution, to avoid production of cyanide gas. Sodium cyanide stock (100 mM) was prepared in PBS adjusted to pH 9.0 with added 4M NaOH. All aqueous solutions contain 0.005% (v/v) of the surfactant Tween-20 and water was of MilliQ quality. TEM Grids were obtained from Pelco International (carbon coated copper grid, cat # 01824, Ted Pella). Sephadex G25 Fine was obtained from SciMed (Asia) Pte Ltd (Singapore). Econo-Pac 1.5x14 cm chromatography columns were obtained from Bio-Rad Laboratories (Singapore) Pte Ltd (Singapore).

UV-vis, TEM, and nanoparticle tracking analysis methods

UV-vis / NIR absorption spectra were recorded at room temperature using a SpectraMax 384 Plus spectrophotometer (Molecular Devices, Wokingham, UK) using a 1 cm path-length quartz cuvette, and a fixed slit width of 2 nm. Transmission Electron Microscopy was performed using a Philips 300CM high-resolution analytical TEM/SEM. Obtained images were not digitally modified other than where necessary to copy the scale bar into image view. Manual analysis of the NR lengths was by use of ImageJ software. Nanoparticle tracking analysis from recorded video images (60 secs) was used to calculate the apparent size of particles in solution in real-time, using a NanoSight LM14 darkfield microscope (Malvern Ltd, UK), sCMOS camera and NTA software v3.1. The LM14 laser unit was equipped with a 532 nm CW laser at 60 mW. NTA setting used for recorded video images were: camera level = 5, shutter = 100, gain = 200, detection threshold = 5, blur = 2-pass, temperature = 25°C, viscosity = water (0.9 cP). The modal size was calculated using the finite track length adjustment (FTLA) algorithm, and data expressed as the arithmetic mean +/- standard error from five different locations within each sample. Size calibration was performed using 100 nm polystyrene nanoparticles (NanoSight Ltd) and obtained a mode of 97.5 +/- 0.4 nm for the population. It is noted that the calculated size of NRs is the average size of nanorods based upon the Brownian motion effect upon NRs of different length/width, which is sufficient for the comparison between mono / polydisperse particle analysis. To ensured maximum discrimination of tracked particles, the NTA software threshold value for counting and tracking particles was kept constant throughout the experiment at a low value (threshold value of 5) to allow a near maximum detection of nanorods.

Nanorod synthesis

Initial experiments used laboratory synthesised nanorods. In a typical procedure, gold seeds were prepared by adding 250 μL of 0.01 M gold (III) chloride solution to 9.75 ml of 0.1 M CTAB solution (30 ℃, in the dark) and continually stirred (500 rpm) before addition of 600 μL of freshly prepared ice-cold 0.01 M $NaBH_4$ solution. Stirring was continued for 2 min, and the reaction was left to stand for 3 hrs. Gold seeds were diluted 1/50 with 0.1 M CTAB solution. Gold nanorods were prepared by adding to 4.75 ml of 0.1 M CTAB solution (30 ℃, in the dark, continuous stirring at 500 rpm) in order, 250 μL of 0.01 M gold (III) chloride solution, 50 μL of 0.01 M silver nitrate solution, 5 μL of 1.0 M HCl, and 35 μL of 0.1 M ascorbic acid solution. 45μL of diluted gold seed solution was added and stirring continued for 30 secs before leaving to stand overnight.

Nanorod Coating and Purification

H-CALNN-OH was prepared at 4 mM in water. H-CVVVT-ol and H-CVVVT-tetra(ethyleneglycol) peptide stock solutions were prepared at 4 mM in 25:75% dimethylsulfoxide (DMSO):MilliQ-quality purified water. Stock dilution was with water. HS-$(CH_2)_{11}$-EG_6 stocks at 100 mM in ethanol were first diluted to 5 mM in ethanol and then to 2 mM with water. All stocks were kept as aliquots at -20 ˚C. Nanorod stocks stored at 4 ˚C tend to have large quantities of precipitated CTAB. This was removed by centrifugation of the nanorods for 1 min at 500 rcf, and repeated if required. Nanorod stock dilutions used for coating samples were that with λ_{max} wavelength absorbance between 0.5 and 1. Self-assembled monolayers on nanorods were formed by adding ten volumes of stock nanorods to one volume of 1 mM coating ligand. The nanoparticle solutions were mixed gently overnight to allow self-assembly of the ligand shell. Purification to remove unreacted ligands, salts and CTAB molecules were performed by one of two methods. For the centrifugation method, an Eppendorf 5418 centrifuge with 7.7 cm radius rotor was used at 5000 rcf for 1 h; the obtained nanorod pellets were resuspended in water. For the chromatography method, Sephadex G25 size-exclusion chromatography was used with a mobile phase of 100 mM NaCl and 0.005 %(v/v) Tween-20.

Electrolyte-Induced Aggregation and DTT-induced Aggregation

To 90 μl of NRs with λ_{max} wavelength absorbance ~ 0.5 was added 10 μl of 100 mM or 400 mM of NaCl solution for 4 h before measurement of UV-vis / NIR spectra. For DTT-induced aggregation, freshly capped NRs (i.e. not purified) were incubated with either 1mM DTT, or 1mM DTT and 100mM NaCl, for various time points.

Cyanide-Mediated Etching of Nanoparticles

Note that NaCN solution must be kept basic to avoid production of highly toxic cyanide gas. NaCN stock at 100 mM (in PBS, pH 9) was diluted to 10 mM in water. NaCN at 10 mM or lower (diluted in water) was added to ligand-

coated nanorods in 0.5 ml water. Nanorods were left for various time intervals at room temperature before UV-vis / NIR spectra were recorded. Samples analysed by nanoparticle tracking analysis were injected into the Nanosight LM14 sample chamber, time course measurements were from the same injected sample.

Results and Discussion

Stabilisation of gold nanorods with a PEG-peptide

Peptides, peptidols, and/or alkylthiol-EGs have been used successfully to coat and stabilise spherical gold and silver nanoparticles (< 20 nm diameter).[27–34] Larger nanoparticles require their ligand coating to provide a greater steric or electrostatic repulsion between nanoparticles to maintain colloidal stability and limit agglomeration / aggregation processes.[48] Thus, longer ligands may help to stabilise NRs. We tested a range of ligands to determine which would impart the most substantial stability to gold NRs: alkylthiol-EG with six ethylene glycol units (fig. 1a: HS-$(CH_2)_{11}$-EG_6), two peptides that had been used successfully with small nanoparticles, H-CALNN-OH (fig. 1b) and H-CVVVT-ol (fig. 1c) and a H-CVVVT-ol peptidol with four ethylene glycol units at the C-terminus (here onwards referred to as peptide-EG: fig. 1d).

Figure 1a shows that a thioalkyl-ethylene glycol ligand HS-$(CH_2)_{11}$-EG_6 stabilises the NRs at 10 mM NaCl, but not at 40 mM NaCl. The peptide H-CALNN-OH (fig. 1b) imparted poor stability in either 10 mM or 40 mM NaCl. The uncharged N-terminal peptide H-CVVVT-ol (fig. 1c) was better with good stability with 10 mM NaCl. At 40 mM NaCl, the UV-vis at higher wavelengths does show some broadening. The peptide-EG ligand H-CVVVT-EG_4 (fig. 1d) showed good stability at both 10 mM and 40 mM NaCl. We used Sephadex G-25 size-exclusion chromatography to successfully remove CTAB and excess coating ligands from the peptide-EG coated NRs (fig 1e). This gave NRs with a slightly shifted λmax when the NRs were in 100 mM NaCl or PBS (pH 7.4). The success of this method depended on the quality of the NRs and the presence of excess CTAB. Until this point in-house synthesised NRs were used, however, commercial CTAB-coated NRs (NanoPartz Inc.) were used in subsequent experiments, as they were more consistent, so enabled improvements in NR purification and stabilisation. Removing excess CTAB in solution (by centrifugation (5,000 rcf, 1h) or size-exclusion chromatography on Sephadex G25 in water) was also performed. HS-$(CH_2)_{11}$-EG_6 ligand was considered to be of a similar length ligand to peptide-EG. Small thiols such as DTT can be used to probe the surface by studying ligand-exchange mediated aggregation of NRs. Freshly coated and unpurified NRs were used, as HS-$(CH_2)_{11}$-EG_6 coated NRs stuck to our G25 columns or pelleted irreversibly upon centrifugation. Within 3 h, HS-$(CH_2)_{11}$-EG_6 coated NRs aggregate in the presence of 1mM DTT (fig S1a). When 100 mM NaCl is added, aggregation is almost instant (fig S1b), again confirming the instability of these NRs to electrolyte (fig 1a). Under the same conditions, peptide-EG NRs were more stable to DTT, not aggregating over the course of 3 hours (fig S1c), though even these aggregate within 2 h in the additional presence of NaCl (fig S1d).

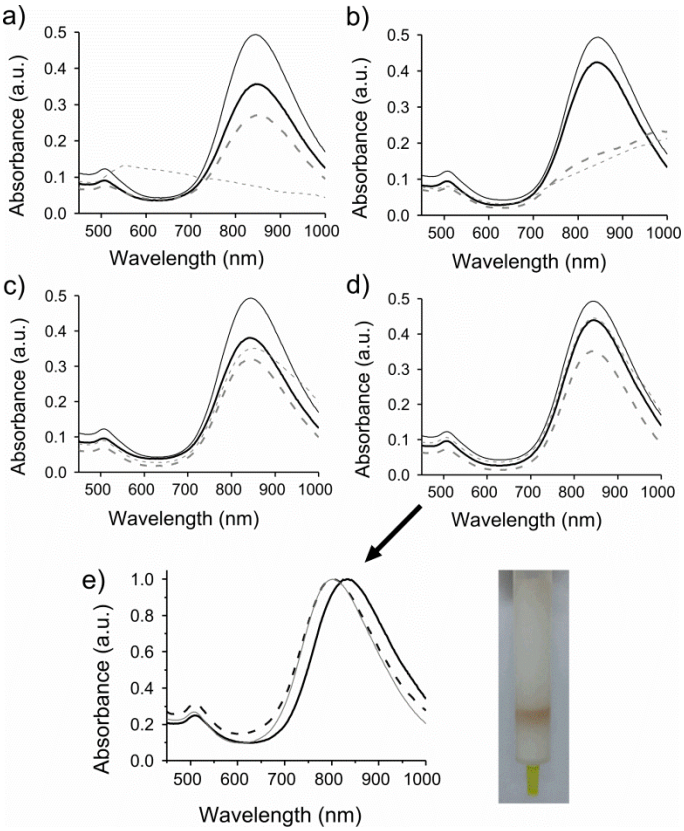

Figure 1: Ligand coating of CTAB-stabilized NRs. (a-d) Spectra of CTAB NRs (thick black lines) and coated NRs (thin black lines) are compared with coated NR solutions containing 10 mM NaCl (dashed lines) or 40 mM NaCl (dotted lines) for 4 h. Coating ligands used were: a) HS-$(CH_2)_{11}$-EG_6, b) H-CALNN-OH, c) H-CVVVT-OH, and d) H-CVVVT-EG_4 (peptide-EG). e) Purification of peptide-EG coated NRs using Sephadex G25 chromatography (image).

Cyanide-mediated etching of peptide-EG nanorods

Etching of CTAB NRs by cyanide ions results in a reduction of their UV-vis / NIR absorption, and eventual their dissolution,[35,36] but this can be prevented/reduced by ligand shells that impart good stability.[14–22] Figure 2a shows the etching effect of sodium cyanide (2 mM) on 602 nm λ_{max} and 842 nm λ_{max} CTAB-stabilized NRs. As expected, CTAB-stabilized NRs (fig. 2a) were rapidly dissolved by cyanide ions, demonstrated by the time-dependent decrease of their plasmon peaks (figs 2b, c), with a slight blue-shift in the λ_{max} wavelength, until by 1 h virtually no absorbance was detectable. In contrast, NR coated with peptide-EG (fig. 2d) were far more resistant to dissolution by cyanide ions (figs 2e, f) and after 60 min more than half the absorbance was still evident. Surprisingly, during the slow etching that occurred, the λmax was substantially red-shifted. After 60 min the λ_{max} 602 NRs has a λ_{max} of 650 nm and after 2 h this was ~700 nm (figs 2b, c), while the λ_{max} 842 NRs has a λ_{max} of 875 nm and ~900 nm at these times (figs 2e, f). While this etching reduced the amplitude of the absorbance, its slow kinetics could provide an opportunity to use etching as a means to modulate λ_{max} of the NR.

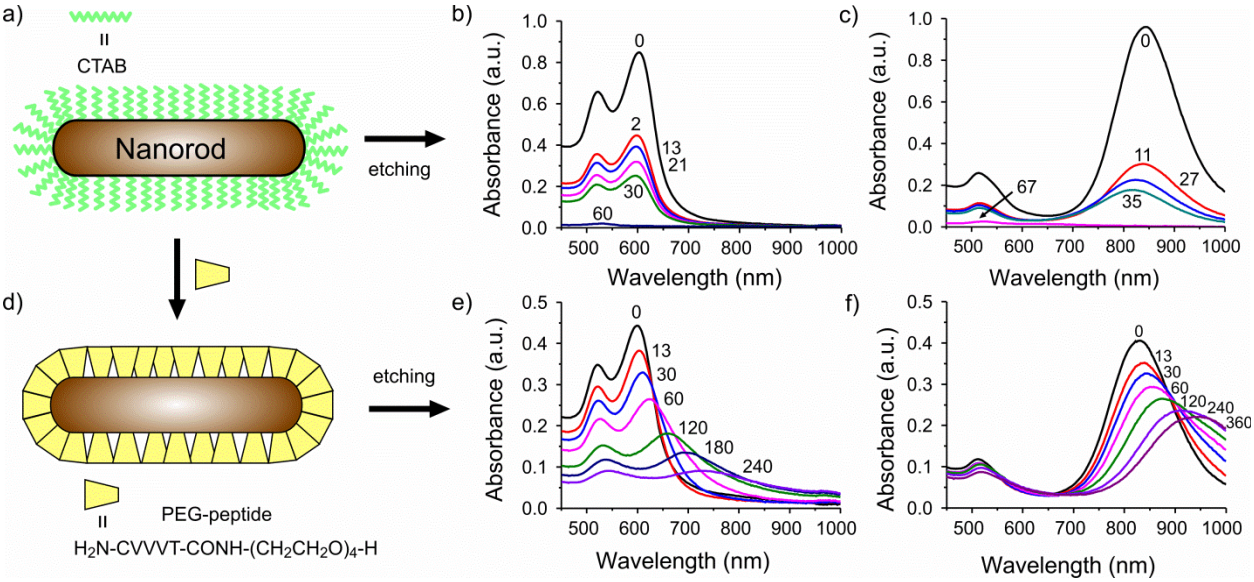

Figure 2: Etching effect on CTAB coated (a) and peptide-EG coated (d) nanorods. Sodium cyanide was added to two different sized CTAB coated gold nanorods (b, c), or two different sized peptide-EG coated gold nanorods (e, f). Numbers indicate the time (min) of nanorods with sodium cyanide.

Such a red-shift may be due to two mechanisms: i) a change in the NR aspect ratio, or ii) NR aggregation / agglomeration. TEM analysis of peptide-EG coated NRs subjected to cyanide (10 mM, 2 h) etching showed pit formation in the NR transverse axis (figure 3a); these NRs displayed a λ_{max} red-shift in the UV-vis / NIR spectra (figure 3b) similar to that in figure 2f. Some of the NRs also show in the TEM a flattening of the ends of the NRs, however analysis of the length of the NRs before cyanide addition (25 rods counted from TEM, length = 76.1 nm +/- 7.1 nm) and after cyanide addition (some TEM samples as shown in figure 3a, 70 rods counted, length = 76.1 nm +/- 6.8 nm) showed no change in average length. The formed pits are most likely due to a less fully coated peptide-EG layer on the NR sides compared to the good coating at the ends (fig. 3c-i). The NR sides are either completely coated with peptide-EG molecules, but the resulting self-assembled monolayer has substantial defects (fig. 3c-ii), or the sides may contain a mix of the peptide-EG and CTAB molecules (fig. 3c-iii) again leading to gaps in the surface coating. A method utilised previously to test for the neutrality of surface charge of a coating (binding to ion-exchange resins) was attempted with the peptide-EG-coated nanorods (data not shown). Results were inconclusive, some batches showed almost complete resistance to binding ion-exchange resins (CM-Sepharose and DEAE-Sepharose), while some batches partially or mostly bound to ion-exchange resins irreversibly even in the presence of 100 mM NaCl. We concluded that a mix of structures, as illustrated in fig 3c-ii and fig 3c-iii were likely and that the balance between species is dependent on some parameter, which is at present not controlled fully. The large decrease in λ_{max} absorbance could be due to etching-mediated dissolution of nanorods, a broadband absorbance of the axially-etched nanorods (due to a mix of NR aspect ratios), or a contribution from aggregation/agglomeration. There is some evidence for the change in λ_{max} being caused by a change in aspect ratio. Thus, a small change in the aspect ratio if measurable and this is in the range required for the observed increases in λ_{max}. It should be noted that this conclusion is mitigated by the high sensitivity of λ_{max} to aspect ratio and the relatively high spread of values of aspect ratios (fig S2 and table S1). Further analysis for the λ_{max} absorbance decrease was done by particle sizing of the cyanide-treated peptide-EG coated NRs in solution during the etching process, using nanoparticle tracking analysis (NTA).

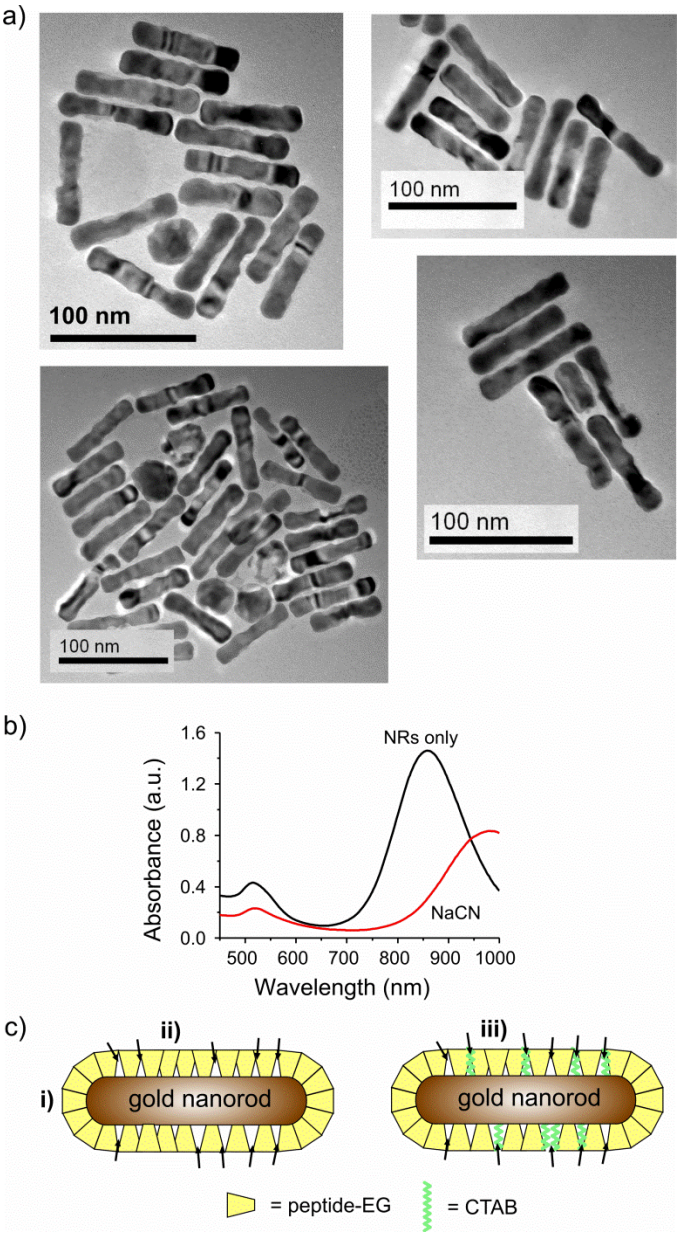

Figure 3: a) TEM of etched peptide-EG coated NRs. b) UV-vis / NIR spectra of the same etched NR sample. c) Schematic of hypothesised surface coating of NRs, with well-coated nanorod ends (c-i) and side coating of peptide-EG only (c-ii) or a mix of peptide-EG and CTAB (c-iii). Arrows illustrate how cyanide could penetrate through an incomplete coating layer.

Nanoparticle tracking analysis of etched peptide-EG nanorods

Etching was analysed in situ at various time points using NTA (830 nm λ_{max} NRs with 10 mM sodium cyanide, 0.1 x PBS, pH 9). Figure 4a shows the modal size vs. concentration of the particle population at various time intervals. During the first 150 min of etching, there was no increase in the modal size of the particles attributable to aggregation, though a slight reduction in apparent size was observed (i.e., NRs moved faster in solution), consistent with a change in aspect ratio. The majority of the particle population (figure 4a) was thus mono-dispersed. At 180 min of etching, there was a dramatic increase in the modal size to 60.1 +/- 0.5 nm. No further analysis of this population was obtained, but it was considered the start of a particle aggregation process. Data for NRs before adding cyanide was not included in figure 4a, however, in an analogous experiment, peptide-EG coated

NRs suspended in water had a modal size of 44.5 +/- 0.2 nm. Figure 4b shows the raw data (no FTLA applied, concentration normalised) to also confirm the shift in the particle population size at 180 min (red line, other lines 150 min or less). Figure 4a also shows that during the etching process, the concentration reduced. The concentration decrease may have been due to etching of less resistant NRs (which were dissolved) or gradual formation of aggregates. Figure 4c shows the size vs. concentration histograms for three time points (5, 120 and 180 mins). With increased time the number of aggregates also increase, however, the population size of these aggregates, even for 180 mins, was very small compared to the modal sized population. How much of a contribution that aggregates play to the decrease in NR concentration cannot yet be quantified. NanoSight NTA also recorded the particle scattering intensity data and confirms these conclusions (fig S3).

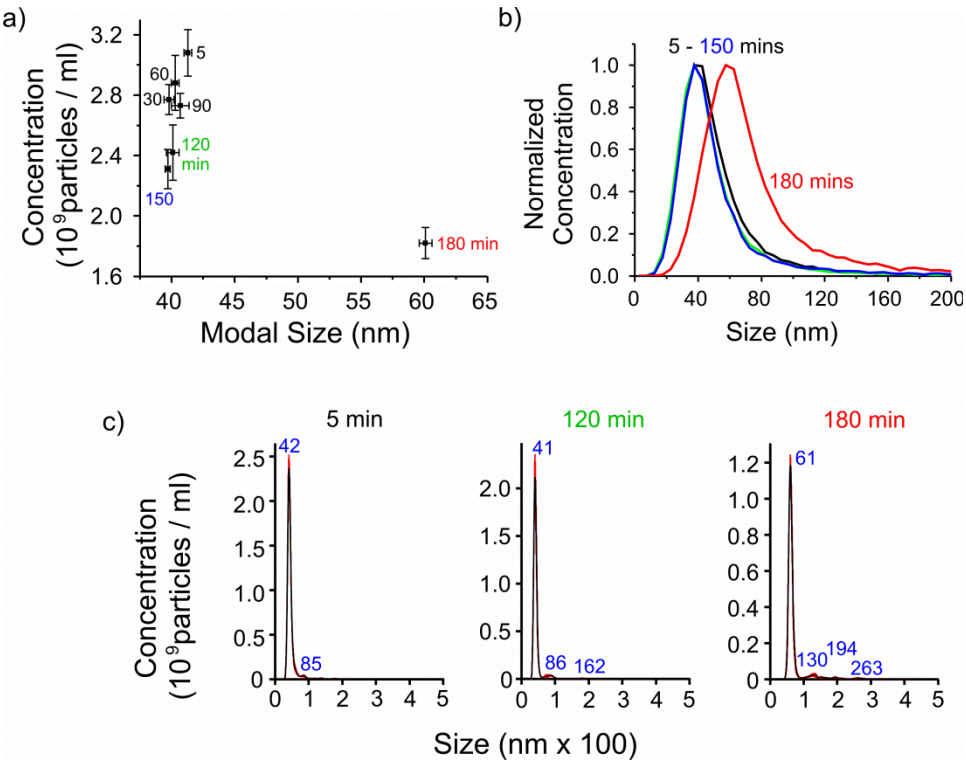

Figure 4: Nanoparticle tracking analysis of peptide-coated gold nanorods during etching. a) FTLA-calculated modal size of NRs vs. concentration. Error bars indicate mean +/- SE of the mode (x-axis) and particle concentration (y-axis) from 5 separate locations of each sample. b) The modal size vs. normalised concentration for raw data. c) Modal size vs. concentration histogram for three different time points.

Controlled etching of peptide-EG coated nanorods.

As the etching kinetics of the peptide-EG coated NRs was slow and caused a red-shift in λ_{max}, it was of interest to determine if this might be used to adjust the λ_{max} and further improve the stability of the NRs. The reduction of absorbance observed upon exposure of peptide-EG coated NRs to cyanide ions (Figs 2, 3) may simply reflect the gradual dissolution of the NRs, though there may be a sub-population of NRs, which for some reason are poorly coated, and these would contribute to a greater extent to the dissolution, at least at earlier times. We, therefore, included peptide-EG ligand during etching. In analogous experimental circumstances it has been shown that a competition reaction occurs between the etchant and coating ligand,[49] and this may increase the performance of the SAM on the NRs in terms of imparting stability. To demonstration etching control, etching of peptide-EG coated 830 nm λ_{max} NRs with high concentrations of sodium cyanide was used as a benchmark. For this, we combined the data from four experiments of peptide-EG NR etching (two experiments 5 mM NaCN, two with 10 mM NaCN) and calculated the 95% upper and lower confidence intervals. This is shown in figure 5a, as the range between the dashed lines as increase in λ_{max} wavelength (fig. 5a, left graph), or decrease in λ_{max} absorbance (fig. 5a, right graph). Several experiments incubating peptide-EG coated 830 nm λ_{max} NRs with different concentrations

of etchant and peptide-EG were performed, (figure 5a). We found that by reducing the sodium cyanide etchant solution to 2 mM or lower, and the inclusion of at least 0.2 mM peptide-EG, the red-shift could be tuned, from 0 nm to 50 nm (figure 5a, left). Moreover, the decrease of λ_{max} absorbance was significantly retarded in all cases (Fig. 5b). A further example demonstrates the effect of adding peptide-EG into etchant solution. With two different sized peptide-EG coated NRs etched with 10 mM sodium cyanide, the addition of 1 mM peptide-EG at 75 min slowed the increase in λ_{max} wavelength and decrease in λ_{max} absorbance (figure 5b).

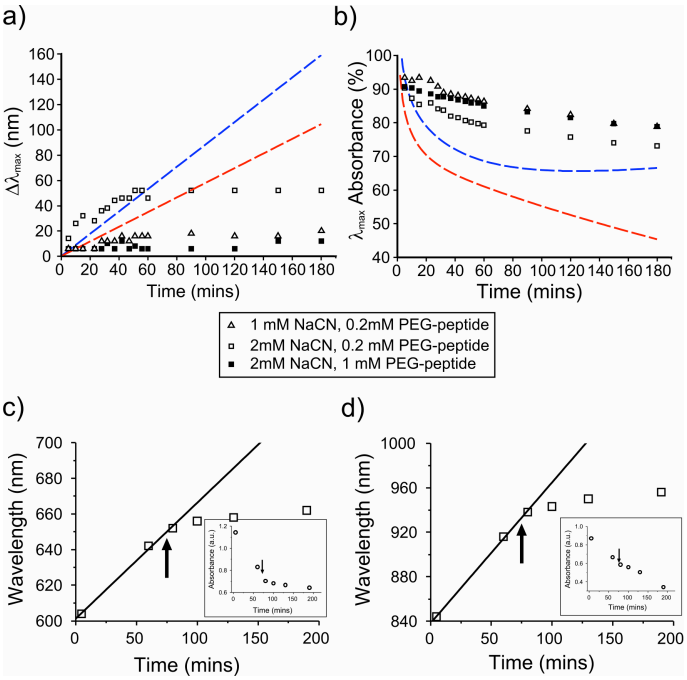

Figure 5: Slowing the etching reaction. The etching effect of NRs on (a) the change in λ_{max} wavelength and (b) decrease in λ_{max} absorbance, in the presence of varied concentrations of peptide-EG and sodium cyanide, are shown. The effect of 5 mM / 10 mM of NaCN on etching peptide-EG NRs is shown as a 95% upper confidence level (dashed blue line) and 95% lower confidence level (dashed red line) for peptide-EG nanorods. The effect of 10 mM etchant and peptide-EG added at 75 min is shown for the change in (c-d) λ_{max} wavelength and (c-d, inserts) λ_{max} absorbance. The solid lines illustrate a linear correlation fit for data between 0 – 80 mins, and arrows are of time when NaCN added.

Conclusion

Here we showed that the peptide-EG ligand was successful in coating gold nanorods and providing good stability in electrolyte solutions such as PBS. To probe the stability further, we subjected the peptide-EG coated NRs to sodium cyanide-mediated etching, which demonstrated the substantially enhanced stability of the coated NRs. We were surprised to observe a red-shift in λ_{max} wavelength over 3 h during etching. TEM analysis showed that the peptide-EG nanorods were transverse etched with the appearance of pits along the longitudinal axis. To further analyse the stability of the peptide-EG NRs, nanoparticle tracking analysis was used to demonstrate that the majority of the nanorods were mono-dispersed up to 150 min of etching. Control over the red-shift caused by the etching reaction could be achieved by changing the etchant concentration and addition of peptide-EG ligand into the reaction. The latter increased the stability of the NRs further. Nanorod biosensor and biotechnology applications[4–12] have a high sensitivity to the environment and molecules attaching to or close to the surface of NRs. Maintaining a high sensitivity is possible with the use of peptide-EG nanorods as they have both a thin coating on the surface and have non-charged surface groups to limit non-specific binding of unwanted molecules. Peptide-EG nanorods will be simple to functionalize and so likely to be useful in at least some biosensor and biotechnology applications.

Acknowledgements

This work has been supported by the Agency for Science, Technology and Research (A*STAR) (PF, WS). DGF acknowledges the support of North West Cancer Research and the Cancer and Polio Research Fund.

References

[1] J. Pérez-Juste, I. Pastoriza-Santos, L. M. Liz-Marzán, P. Mulvaney, Coord. Chem. Rev. 249 (2005) 1870–1901. doi:10.1016/j.ccr.2005.01.030.

[2] C.J. Murphy, L.B. Thompson, A.M. Alkilany, P.N. Sisco, S.P. Boulos, S.T. Sivapalan, J. A. Yang, D. J. Chernak, J. Huang, J. Phys. Chem. Lett. 1 (2010) 2867–2875. doi:10.1021/jz100992x.

[3] H. Chen, L. Shao, Q. Li, J. Wang, Chem. Soc. Rev. 42 (2013) 2679–2724. doi:10.1039/C2CS35367A.

[4] M. Eghtedari, M. Motamedi, V.L. Popov, N.A. Kotov, A.A. Oraevsky, in: A.A. Oraevsky, L. V. Wang (Eds.), SPIE Proceedings - Photons Plus Ultrasound Imaging Sens., 2004: pp. 21–28. doi:10.1117/12.534464.

[5] L. Tong, Q. Wei, A. Wei, J. Cheng, Photochem. Photobiol. 85 (2009) 21–32.

[6] X. Huang, M. a. El-Sayed, J. Adv. Res. 1 (2010) 13–28. doi:10.1016/j.jare.2010.02.002.

[7] X. Huang, M. a. El-Sayed, Alexandria J. Med. 47 (2011) 1–9. doi:10.1016/j.ajme.2011.01.001.

[8] A.M. Alkilany, L.B. Thompson, S.P. Boulos, P.N. Sisco, C.J. Murphy, Adv. Drug Deliv. Rev. 64 (2012) 190–199. doi:10.1016/j.addr.2011.03.005.

[9] J. Cao, T. Sun, K.T.V. Grattan, Sensors Actuators B Chem. 195 (2014) 332–351. doi:10.1016/j.snb.2014.01.056.

[10] S.C. Boca, S. Astilean, Nanotechnology. 21 (2010) 235601.

[11] Z. Zhang, L. Wang, J. Wang, X. Jiang, X. Li, Z. Hu, Y. Ji, X. Wu, C. Chen, Adv. Mater. 24 (2012) 1349–1349. doi:10.1002/adma.201290063.

[12] Y. Zhang, J. Qian, D. Wang, Y. Wang, S. He, Angew. Chemie Int. Ed. 52 (2013) 1148–1151. doi:10.1002/anie.201207909.

[13] A.M. Alkilany, P.K. Nagaria, C.R. Hexel, T.J. Shaw, C.J. Murphy, M.D. Wyatt, Small. 5 (2009) 701–708. doi:10.1002/smll.200801546.

[14] D. Pissuwan, T. Niidome, Nanoscale. 7 (2015) 59–65. doi:10.1039/C4NR04350B.

[15] D. Gentili, G. Ori, M. Comes Franchini, Chem. Commun. 39 (2009) 5874–6. doi:10.1039/b911582j.

[16] S. Manohar, R. Rayavarapu, W. Petersen, T.G. van Leeuwen, in: A.A. Oraevsky, L. V. Wang (Eds.), SPIE Proc., 2009: p. 71772D. doi:10.1117/12.808547.

[17] M. Liu, W.-C. Law, A. Kopwitthaya, X. Liu, M.T. Swihart, P.N. Prasad, Chem. Commun. 49 (2013) 9350–9352. doi:10.1039/c3cc45103h.

[18] J.G. Mehtala, A. Wei, Langmuir. 30 (2014) 13737–13743. doi:10.1021/la502955h.

[19] Q. Dai, J. Coutts, J. Zou, Q. Huo, Chem. Commun. 7345 (2008) 2858–60. doi:10.1039/b804797a.

[20] Y. Niidome, K. Honda, K. Higashimoto, H. Kawazumi, S. Yamada, N. Nakashima, Y. Sasaki, Y. Ishida, J-I Kikuchi, Chem. Commun. (2007) 3777–9. doi:10.1039/b706671f.

[21] L. Vigderman, P. Manna, E.R. Zubarev, Angew. Chemie - Int. Ed. 51 (2012) 636–41. doi:10.1002/anie.201107304.

[22] Y. Xu, Y. Zhao, L. Chen, X. Wang, J. Sun, H. Wu, F. Bao, J. Fan, Q. Zhang, Nanoscale. 7 (2015) 6790-6797.

[23] D. Bartczak, O.L. Muskens, S. Nitti, T.M. Millar, A.G. Kanaras, Biomater. Sci. 3 (2015) 733–741. doi:10.1039/C5BM00053J.

[24] C. Hamon, T. Bizien, F. Artzner, P. Even-Hernandez, V. Marchi, J. Colloid Interface Sci. 424 (2014) 90–97. doi:10.1016/j.jcis.2014.03.002.

[25] W. He, S. Hou, X. Mao, X. Wu, Y. Ji, J. Liu, X. Hu, K. Zhang, C. Wang, Y. Yang, Q. Wang, Chem. Commun. 47 (2011) 5482. doi:10.1039/c1cc10394f.

[26] W.P. Wuelfing, S.M. Gross, D.T. Miles, R.W. Murray, J. Am. Chem. Soc. 120 (1998) 12696–12697. doi:10.1021/ja983183m.

[27] R. Lévy, N.T.K. Thanh, R. C. Doty, I. Hussain, R.J. Nichols, D.J. Schiffrin, M. Brust, D. G. Fernig, J. Am. Chem. Soc. 126 (2004) 10076–10084. doi:10.1021/ja0487269.

[28] L. Duchesne, D. Gentili, M. Comes-Franchini, D.G. Fernig, Langmuir. 24 (2008) 13572–13580. doi:10.1021/la802876u.

[29] X. Chen, W.W. Qoutah, P. Free, J. Hobley, D.G. Fernig, D. Paramelle, Aust. J. Chem. 65 (2012) 266–274. doi:10.1071/CH11432.
[30] P. Free, D. Paramelle, M. Bosman, J. Hobley, D.G. Fernig, Aust. J. Chem. 65 (2012) 275–282. doi:10.1071/CH11429.
[31] P. Free, C.P. Shaw, R. Lévy, Chem. Commun. (2009) 5009–11. doi:10.1039/b910657j.
[32] V. Sée, P. Free, Y. Cesbron, P. Nativo, U. Shaheen, D.J. Rigden, D. G. Spiller, D. G. Fernig, M. R. H. White, I. A. Prior, M. Brust, B. Lounis, R. Lévy, ACS Nano. 3 (2009) 2461–8. doi:10.1021/nn9006994.
[33] Y. Cesbron, U. Shaheen, P. Free, R. Lévy, PLoS One. 10 (2015) e0121683. doi:10.1371/journal.pone.0121683.
[34] D.J. Nieves, N.S. Azmi, R. Xu, R. Lévy, E.A. Yates, D.G. Fernig, Chem. Commun. 50 (2014) 13157–60. doi:10.1039/c4cc05909c.
[35] N.R. Jana, L. Gearheart, S.O. Obare, C.J. Murphy, Langmuir. 18 (2002) 922–927. doi:10.1021/la0114530.
[36] J. Rodríguez-Fernández, J. Pérez-Juste, P. Mulvaney, L. M. Liz-Marzán, J Phys. Chem. B. 109 (2005) 14257–14261.
[37] Y. Zheng, J. Zeng, A. Ruditskiy, M. Liu, Y. Xia, Chem. Mater. 26 (2014) 22–33. doi:10.1021/cm402023g.
[38] G. Mettela, G.U. Kulkarni, Nano Res. 8 (2015) 2925–2934. doi:10.1007/s12274-015-0797-8.
[39] C.K. Tsung, X. Kou, Q. Shi, J. Zhang, M.H. Yeung, J. Wang, G. D. Stucky, J. Am. Chem. Soc. 128 (2006) 5352–5353. doi:10.1021/ja060447t.
[40] R. Zou, X. Guo, J. Yang, D. Li, F. Peng, L. Zhang, H. Wang, H. Yu, CrystEngComm. 11 (2009) 2797. doi:10.1039/b911902g.
[41] T. Wen, H. Zhang, X. Tang, W. Chu, W. Liu, Y. Ji, Z. Hu, S. Hou, X. Hu, X. Wu, J. Phys. Chem. C. 117 (2013) 25769–25777. doi:10.1021/jp407774s.
[42] Z. Chen, Z. Zhang, C. Qu, D. Pan, L. Chen, Analyst. 137 (2012) 5197. doi:10.1039/c2an35787a.
[43] X. Liu, S. Zhang, P. Tan, J. Zhou, Y. Huang, Z. Nie, S. Yao, Chem. Commun. 49 (2013) 1856–8. doi:10.1039/c3cc38476d.
[44] L. Saa, M. Coronado-Puchau, V. Pavlov, L.M. Liz-Marzán, Nanoscale. 6 (2014) 7405. doi:10.1039/c4nr01323a.
[45] S.A. Alex, J. Satija, M.A. Khan, G.M. Bhalerao, S. Chakravarty, B. Kasilingam, A. Sivakumar, N. Chandrasekaran, A. Mukherjee, Anal. Methods. 7 (2015) 5583–5592. doi:10.1039/C5AY00935A.
[46] L. Duchesne, V. Octeau, R.N. Bearon, A. Beckett, I.A. Prior, B. Lounis, D. G. Fernig, PLoS Biol. 10 (2012) e1001361. doi:10.1371/journal.pbio.1001361.
[47] D.J. Nieves, Y. Li, D.G. Fernig, R. Lévy, R. Soc. Open Sci. 2 (2015) 140454. doi:10.1098/rsos.140454.
[48] L.A. Wijenayaka, M.R. Ivanov, C.M. Cheatum, A.J. Haes, J. Phys. Chem. C. 119 (2015) 10064–10075. doi:10.1021/acs.jpcc.5b00483.
[49] F. Schulz, T. Vossmeyer, N.G. Bastús, H. Weller, Langmuir. 29 (2013) 9897–9908. doi:10.1021/la401956c.

Supplementary Information

Title

High colloidal stability of gold nanorods coated with a peptide-ethylene glycol: analysis by cyanide-mediated etching and nanoparticle tracking analysis.

Paul Free*[a], Gao Conger[b], Wu Siji[a], Jing Bo Zhang[c], David G. Fernig[d].

[a]Institute of Materials Research and Engineering, Agency for Science, Technology & Research (A*STAR), 2 Fusionopolis Way, Innovis, #08-03, Singapore 138634.
[b]Division of Bioengineering and [c]Advanced Environmental & Biotechnology Centre, Nanyang Environment & Water Research Institute, Nanyang Technological University, Singapore 637141.
[d]Department of Biochemistry, Institute of Integrative Biology, University of Liverpool, Liverpool L69 7ZB, UK.
***corresponding author: freepf@imre.a-star.edu.sg**

Supplementary Information

Table of contents

Figure S1: DTT-induced aggregation of coated NRs page 2

Figure S2: Approximation of change of λ_{max} with change in nanorod diameter page 3

Table S1: Approximate λ_{max} of nanorods with different diameters. page 3

Figure S3: Nanoparticle tracking analysis of peptide-EG coated gold nanorods during etching page 4

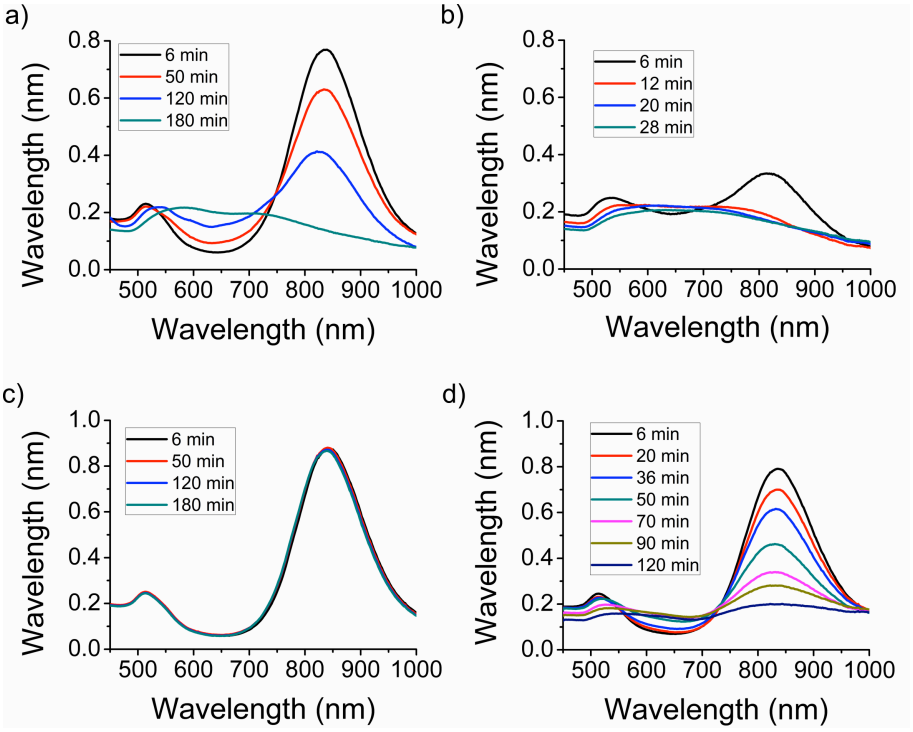

Figure S1: DTT-induced aggregation following coating of NRs. NRs were used without further purification due to HS-$(CH_2)_{11}$-EG_6 coated rods non-specifically binding to Sephadex G25. HS-$(CH_2)_{11}$-EG_6 coated NRs (a,b) and peptide-EG coated NRs (c, d), were treated with a, c) 1 mM DTT or b, d) 1 mM DTT and 100 mM NaCl. UV-vis spectra were acquired at the times indicated. In the absence of additional electrolytes the HS-$(CH_2)_{11}$-EG_6 coated NRs show a change in their UV-vis spectrum by 50 min (a) and by 180 min their plasmon bands are no longer apparent. In contrast, peptide-EG coated NRs showed no change in spectrum (c). In the presence of 1 mM DTT and an additional 100 mM NaCl, the plasmon bands of the $CH_2)_{11}$-EG_6 coated NRs were substantially reduced by 6 min and had disappeared after 12 min (b). With the peptide-EG coated NRs however, the spectrum only began to change after 20 min, and it was only after 120 min that the plasmon bands were no longer apparent (d).

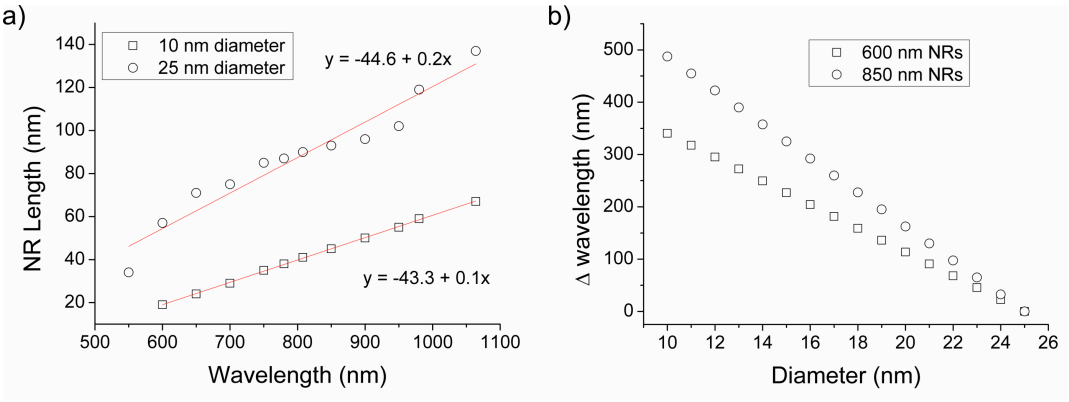

Figure S2: Approximation of change of λ_{max} with a change in nanorod diameter. a) Data obtained online from Nanopartz Inc. (http://www.nanopartz.com/) of 10 nm and 25 nm (CTAB-coated) nanorods. A plot of nanorod λ_{max} wavelength vs. nanorod length gives approximate linear fit correlation (red lines). b) For two fixed length nanorods (with 600 nm and 850 nm λ_{max} wavelengths), the linear correlation between change in nanorod diameter vs. increase in λ_{max} wavelength is shown.

Diameter (nm)	Wavelength (nm)		Diameter (nm)	Wavelength (nm)
25	600		25	850
24	623		24	882
23	645		23	915
22	668		22	947
21	691		21	980
20	713		20	1012

Table S1: Approximate λ_{max} of nanorods with different diameters. The data were obtained from figure S2-b and show the λ_{max} of nanorods with a different diameter and with a fixed length.

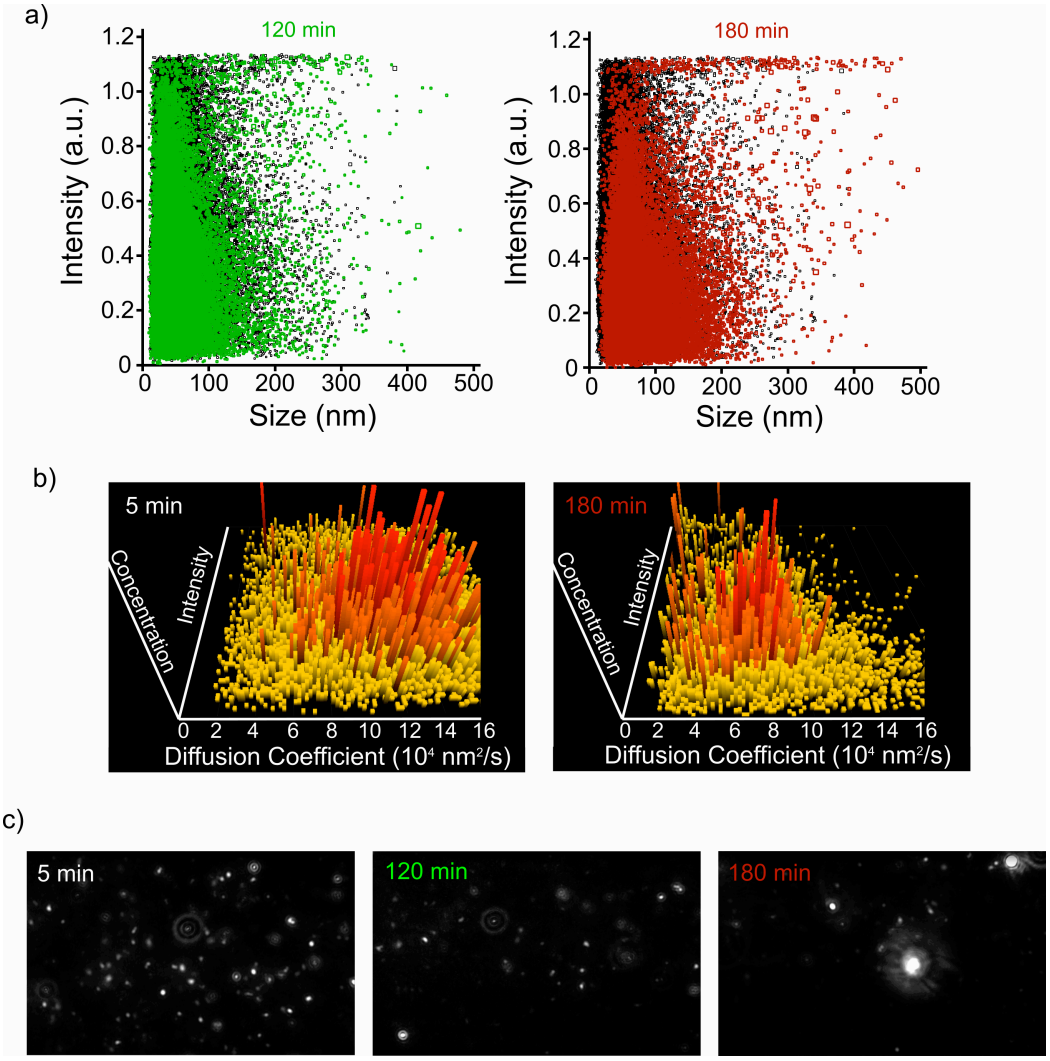

Figure S3: Nanoparticle tracking analysis of peptide-EG coated gold nanorods during etching. a) Modal size vs. particle intensity after 5 min (black boxes), 120 min (green boxes) and 180 min (red boxes) etching. b) Diffusion coefficient vs. intensity vs. concentration histogram plots for the 5 min etched sample (left), and 180 min etched sample (right). c) Example images from recorded tracking analysis videos at 5, 120 and 180 min.